

Improved determination of the sample composition of dimuon events produced in $p\bar{p}$ collisions at $\sqrt{s} = 1.96$ TeV

T. Aaltonen,²¹ B. Álvarez González^{w,9} S. Amerio,⁴⁰ D. Amidei,³¹ A. Anastassov,³⁵ A. Annovi,¹⁷ J. Antos,¹² G. Apollinari,¹⁵ A. Apresyan,⁴⁴ T. Arisawa,⁵⁴ A. Artikov,¹³ J. Asaadi,⁴⁹ W. Ashmanskas,¹⁵ B. Auerbach,⁵⁷ A. Aurisano,⁴⁹ F. Azfar,³⁹ W. Badgett,¹⁵ A. Barbaro-Galtieri,²⁵ V.E. Barnes,⁴⁴ B.A. Barnett,²³ P. Barria^{dd,42} P. Bartos,¹² M. Baucé^{bb,40} F. Bedeschi,⁴² D. Beecher,²⁷ S. Behari,²³ G. Bellettini^{cc,42} J. Bellinger,⁵⁶ D. Benjamin,¹⁴ A. Beretvas,¹⁵ A. Bhatti,⁴⁶ M. Binkley^{*,15} D. Bisello^{bb,40} I. Bizjak^{hh,27} K.R. Bland,⁵ B. Blumenfeld,²³ A. Bocci,¹⁴ A. Bodek,⁴⁵ D. Bortoletto,⁴⁴ J. Boudreau,⁴³ A. Boveia,¹¹ B. Brau^{a,15} L. Brigliadori^{aa,6} A. Brisuda,¹² C. Bromberg,³² E. Brucken,²¹ M. Bucciantonio^{cc,42} J. Budagov,¹³ H.S. Budd,⁴⁵ S. Budd,²² K. Burkett,¹⁵ G. Busetto^{bb,40} P. Bussey,¹⁹ A. Buzatu,³⁰ C. Calancha,²⁸ S. Camarda,⁴ M. Campanelli,³² M. Campbell,³¹ F. Canelli^{11,15} B. Carls,²² D. Carlsmith,⁵⁶ R. Carosi,⁴² S. Carrillo^{k,16} S. Carron,¹⁵ B. Casal,⁹ M. Casarsa,¹⁵ A. Castro^{aa,6} P. Catastini,²⁰ D. Cauz,⁵⁰ V. Cavaliere,²² M. Cavalli-Sforza,⁴ A. Cerri^{f,25} L. Cerrito^{g,27} Y.C. Chen,¹ G. Chiarelli,⁴² G. Chlachidze,¹⁵ F. Chlebana,¹⁵ K. Cho,²⁴ D. Chokheli,¹³ J.P. Chou,²⁰ W.H. Chung,⁵⁶ Y.S. Chung,⁴⁵ C.I. Ciobanu,⁴¹ M.A. Ciocci^{dd,42} A. Clark,¹⁸ C. Clarke,⁵⁵ G. Compostella^{bb,40} M.E. Convery,¹⁵ M. Corbo,⁴¹ M. Cordelli,¹⁷ C.A. Cox,⁷ D.J. Cox,⁷ F. Crescioli^{cc,42} C. Cuenca Almenar,⁵⁷ J. Cuevas^{w,9} D. Dagenhart,¹⁵ N. d'Ascenzo^{u,41} M. Datta,¹⁵ P. de Barbaro,⁴⁵ S. De Cecco,⁴⁷ G. De Lorenzo,⁴ M. Dell'Orso^{cc,42} C. Deluca,⁴ L. Demortier,⁴⁶ J. Deng^{c,14} M. Deninno,⁶ F. Devoto,²¹ M. d'Errico^{bb,40} A. Di Canto^{cc,42} B. Di Ruzza,⁴² J.R. Dittmann,⁵ M. D'Onofrio,²⁶ S. Donati^{cc,42} P. Dong,¹⁵ M. Dorigo,⁵⁰ T. Dorigo,⁴⁰ K. Ebina,⁵⁴ A. Elagin,⁴⁹ A. Eppig,³¹ R. Erbacher,⁷ D. Errede,²² S. Errede,²² N. Ershaidat^{z,41} R. Eusebi,⁴⁹ H.C. Fang,²⁵ J.P. Fernandez,²⁸ C. Ferrazza^{ee,42} R. Field,¹⁶ G. Flanagan^{s,44} R. Forrest,⁷ M.J. Frank,⁵ M. Franklin,²⁰ J.C. Freeman,¹⁵ Y. Funakoshi,⁵⁴ I. Furic,¹⁶ M. Gallinaro,⁴⁶ J. Galyardt,¹⁰ J.E. Garcia,¹⁸ A.F. Garfinkel,⁴⁴ P. Garosi^{dd,42} H. Gerberich,²² E. Gerchtein,¹⁵ S. Giagu^{ff,47} V. Giakoumopoulou,³ P. Giannetti,⁴² K. Gibson,⁴³ C.M. Ginsburg,¹⁵ N. Giokaris,³ P. Giromini,¹⁷ M. Giunta,⁴²

* Deceased

G. Giurgiu,²³ V. Glagolev,¹³ D. Glenzinski,¹⁵ M. Gold,³⁴ D. Goldin,⁴⁹ N. Goldschmidt,¹⁶
 A. Golossanov,¹⁵ G. Gomez,⁹ G. Gomez-Ceballos,²⁹ M. Goncharov,²⁹ O. González,²⁸
 I. Gorelov,³⁴ A.T. Goshaw,¹⁴ K. Goulianos,⁴⁶ S. Grinstein,⁴ C. Grosso-Pilcher,¹¹
 R.C. Group^{53,15} J. Guimaraes da Costa,²⁰ Z. Gunay-Unalan,³² C. Haber,²⁵ S.R. Hahn,¹⁵
 E. Halkiadakis,⁴⁸ A. Hamaguchi,³⁸ J.Y. Han,⁴⁵ F. Happacher,¹⁷ K. Hara,⁵¹ D. Hare,⁴⁸
 M. Hare,⁵² R.F. Harr,⁵⁵ K. Hatakeyama,⁵ M. Herndon,⁵⁶ S. Hewamanage,⁵ D. Hidas,⁴⁸
 A. Hocker,¹⁵ W. Hopkins^{g,15} S. Hou,¹ R.E. Hughes,³⁶ M. Hurwitz,¹¹ U. Husemann,⁵⁷
 N. Hussain,³⁰ M. Hussein,³² J. Huston,³² G. Introzzi,⁴² M. Iori^{ff,47} A. Ivanov^{o,7} D. Jang,¹⁰
 B. Jayatilaka,¹⁴ E.J. Jeon,²⁴ M.K. Jha,⁶ S. Jindariani,¹⁵ W. Johnson,⁷ M. Jones,⁴⁴
 K.K. Joo,²⁴ S.Y. Jun,¹⁰ T.R. Junk,¹⁵ T. Kamon,⁴⁹ A. Kasmi,⁵ Y. Kato^{n,38} W. Ketchum,¹¹
 V. Khotilovich,⁴⁹ B. Kilminster,¹⁵ D.H. Kim,²⁴ H.S. Kim,²⁴ H.W. Kim,²⁴ J.E. Kim,²⁴
 M.J. Kim,¹⁷ S.B. Kim,²⁴ S.H. Kim,⁵¹ Y.K. Kim,¹¹ N. Kimura,⁵⁴ M. Kirby,¹⁵ S. Klimentko,¹⁶
 K. Kondo,⁵⁴ D.J. Kong,²⁴ J. Konigsberg,¹⁶ D. Krop,¹¹ N. Krumnack^{l,5} M. Kruse,¹⁴
 V. Krutelyov^{d,49} M. Kurata,⁵¹ S. Kwang,¹¹ A.T. Laasanen,⁴⁴ S. Lami,⁴² S. Lammel,¹⁵
 M. Lancaster,²⁷ R.L. Lander,⁷ K. Lannon^{v,36} A. Lath,⁴⁸ G. Latino^{cc,42} E. Lee,⁴⁹ H.S. Lee,¹¹
 J.S. Lee,²⁴ S.W. Lee^{x,49} S. Leo^{cc,42} S. Leone,⁴² J.D. Lewis,¹⁵ A. Limosani^{r,14} C.-J. Lin,²⁵
 J. Linacre,³⁹ M. Lindgren,¹⁵ A. Lister,¹⁸ D.O. Litvintsev,¹⁵ C. Liu,⁴³ Q. Liu,⁴⁴ T. Liu,¹⁵
 S. Lockwitz,⁵⁷ A. Loginov,⁵⁷ D. Lucchesi^{bb,40} P. Lujan,²⁵ P. Lukens,¹⁵ G. Lungu,⁴⁶ J. Lys,²⁵
 R. Lysak,¹² R. Madrak,¹⁵ K. Maeshima,¹⁵ K. Makhoul,²⁹ S. Malik,⁴⁶ G. Manca^{b,26}
 A. Manousakis-Katsikakis,³ F. Margaroli,⁴⁴ M. Martínez,⁴ R. Martínez-Ballarín,²⁸
 P. Mastrandrea,⁴⁷ M.E. Mattson,⁵⁵ P. Mazzanti,⁶ K.S. McFarland,⁴⁵ P. McIntyre,⁴⁹
 R. McNulty^{i,26} A. Mehta,²⁶ P. Mehtala,²¹ A. Menzione,⁴² C. Mesropian,⁴⁶ T. Miao,¹⁵
 D. Mietlicki,³¹ A. Mitra,¹ H. Miyake,⁵¹ S. Moed,²⁰ N. Moggi,⁶ M.N. Mondragon^{k,15}
 C.S. Moon,²⁴ R. Moore,¹⁵ M.J. Morello,¹⁵ P. Movilla Fernandez,¹⁵ A. Mukherjee,¹⁵
 M. Mussini^{aa,6} J. Nachtman^{m,15} Y. Nagai,⁵¹ J. Naganoma,⁵⁴ I. Nakano,³⁷ A. Napier,⁵²
 J. Nett,⁴⁹ C. Neu,⁵³ M.S. Neubauer,²² J. Nielsen^{e,25} O. Norriella,²² E. Nurse,²⁷ L. Oakes,³⁹
 S.H. Oh,¹⁴ Y.D. Oh,²⁴ I. Oksuzian,⁵³ T. Okusawa,³⁸ R. Orava,²¹ L. Ortolan,⁴
 S. Pagan Griso^{bb,40} C. Pagliarone,⁵⁰ E. Palencia^{f,9} V. Papadimitriou,¹⁵ J. Patrick,¹⁵
 G. Pauletta^{gg,50} C. Paus,²⁹ D.E. Pellett,⁷ A. Penzo,⁵⁰ T.J. Phillips,¹⁴ G. Piacentino,⁴²
 J. Pilot,³⁶ K. Pitts,²² C. Plager,⁸ L. Pondrom,⁵⁶ K. Potamianos,⁴⁴ O. Poukhov^{*,13}

F. Prokoshin^{y,13} A. Pronko,¹⁵ F. Ptohos^{h,17} E. Pueschel,¹⁰ G. Punzi^{cc,42} J. Pursley,⁵⁶
A. Rahaman,⁴³ V. Ramakrishnan,⁵⁶ N. Ranjan,⁴⁴ I. Redondo,²⁸ M. Rescigno,⁴⁷
T. Riddick,²⁷ F. Rimondi^{aa,6} L. Ristori^{42,15} T. Rodrigo,⁹ E. Rogers,²² S. Rolli,⁵² R. Roser,¹⁵
M. Rossi,⁵⁰ F. Rubbo,¹⁵ F. Ruffini^{dd,42} A. Ruiz,⁹ J. Russ,¹⁰ V. Rusu,¹⁵ A. Safonov,⁴⁹
W.K. Sakumoto,⁴⁵ Y. Sakurai,⁵⁴ L. Santi^{gg,50} L. Sartori,⁴² K. Sato,⁵¹ V. Saveliev^{u,41}
A. Savoy-Navarro,⁴¹ P. Schlabach,¹⁵ E.E. Schmidt,¹⁵ M.P. Schmidt^{*,57} M. Schmitt,³⁵
T. Schwarz,⁷ L. Scodellaro,⁹ A. Scribano^{dd,42} F. Scuri,⁴² A. Sedov,⁴⁴ S. Seidel,³⁴ Y. Seiya,³⁸
A. Semenov,¹³ F. Sforza^{cc,42} A. Sfyrla,²² S.Z. Shalhout,⁷ T. Shears,²⁶ P.F. Shepard,⁴³
M. Shimojima^{t,51} S. Shiraishi,¹¹ M. Shochet,¹¹ I. Shreyber,³³ A. Simonenko,¹³
P. Sinervo,³⁰ A. Sissakian^{*,13} K. Sliwa,⁵² J.R. Smith,⁷ F.D. Snider,¹⁵ A. Soha,¹⁵
S. Somalwar,⁴⁸ V. Sorin,⁴ P. Squillacioti,¹⁵ M. Stancari,¹⁵ M. Stanitzki,⁵⁷ R. St. Denis,¹⁹
B. Stelzer,³⁰ O. Stelzer-Chilton,³⁰ D. Stentz,³⁵ J. Strologas,³⁴ G.L. Strycker,³¹ Y. Sudo,⁵¹
A. Sukhanov,¹⁶ I. Suslov,¹³ K. Takemasa,⁵¹ Y. Takeuchi,⁵¹ J. Tang,¹¹ M. Tecchio,³¹
P.K. Teng,¹ J. Thom^{g,15} J. Thome,¹⁰ G.A. Thompson,²² P. Ttito-Guzmán,²⁸ S. Tkaczyk,¹⁵
D. Toback,⁴⁹ S. Tokar,¹² K. Tollefson,³² T. Tomura,⁵¹ S. Torre,¹⁷ D. Torretta,¹⁵
P. Totaro,⁴⁰ M. Trovato^{ee,42} F. Ukegawa,⁵¹ S. Uozumi,²⁴ A. Varganov,³¹ F. Vázquez^{k,16}
G. Velev,¹⁵ C. Vellidis,³ M. Vidal,²⁸ I. Vila,⁹ R. Vilar,⁹ J. Vizán,⁹ M. Vogel,³⁴ G. Volpi^{cc,42}
R.L. Wagner,¹⁵ T. Wakisaka,³⁸ R. Wallny,⁸ S.M. Wang,¹ A. Warburton,³⁰ D. Waters,²⁷
M. Weinberger,⁴⁹ B. Whitehouse,⁵² A.B. Wicklund,² E. Wicklund,¹⁵ S. Wilbur,¹¹
J.S. Wilson,³⁶ P. Wilson,¹⁵ B.L. Winer,³⁶ P. Wittich^{g,15} S. Wolbers,¹⁵ H. Wolfe,³⁶
T. Wright,³¹ X. Wu,¹⁸ Z. Wu,⁵ K. Yamamoto,³⁸ J. Yamaoka,¹⁴ T. Yang,¹⁵ U.K. Yang^{p,11}
Y.C. Yang,²⁴ W.-M. Yao,²⁵ G.P. Yeh,¹⁵ K. Yi^{m,15} J. Yoh,¹⁵ K. Yorita,⁵⁴ T. Yoshida^{j,38}
G.B. Yu,¹⁴ I. Yu,²⁴ S.S. Yu,¹⁵ J.C. Yun,¹⁵ A. Zanetti,⁵⁰ Y. Zeng,¹⁴ and S. Zucchelli^{aa6}

(CDF Collaboration[†])

[†] With visitors from ^aUniversity of MA Amherst, Amherst, MA 01003, USA, ^bIstituto Nazionale di Fisica Nucleare, Sezione di Cagliari, 09042 Monserrato (Cagliari), Italy, ^cUniversity of CA Irvine, Irvine, CA 92697, USA, ^dUniversity of CA Santa Barbara, Santa Barbara, CA 93106, USA, ^eUniversity of CA Santa Cruz, Santa Cruz, CA 95064, USA, ^fCERN, CH-1211 Geneva, Switzerland, ^gCornell University, Ithaca, NY 14853, USA, ^hUniversity of Cyprus, Nicosia CY-1678, Cyprus, ⁱUniversity College Dublin, Dublin 4, Ireland, ^jUniversity of Fukui, Fukui City, Fukui Prefecture, Japan 910-0017, ^kUniversidad Iberoamericana, Mexico D.F., Mexico, ^lIowa State University, Ames, IA 50011, USA, ^mUniversity of Iowa, Iowa

- ¹*Institute of Physics, Academia Sinica,
Taipei, Taiwan 11529, Republic of China*
- ²*Argonne National Laboratory, Argonne, Illinois 60439, USA*
- ³*University of Athens, 157 71 Athens, Greece*
- ⁴*Institut de Fisica d'Altes Energies, ICREA,
Universitat Autònoma de Barcelona,
E-08193, Bellaterra (Barcelona), Spain*
- ⁵*Baylor University, Waco, Texas 76798, USA*
- ⁶*Istituto Nazionale di Fisica Nucleare Bologna,
^{aa}University of Bologna, I-40127 Bologna, Italy*
- ⁷*University of California, Davis, Davis, California 95616, USA*
- ⁸*University of California, Los Angeles,
Los Angeles, California 90024, USA*
- ⁹*Instituto de Fisica de Cantabria, CSIC-University of Cantabria, 39005 Santander, Spain*
- ¹⁰*Carnegie Mellon University, Pittsburgh, Pennsylvania 15213, USA*
- ¹¹*Enrico Fermi Institute, University of Chicago, Chicago, Illinois 60637, USA*
- ¹²*Comenius University, 842 48 Bratislava,
Slovakia; Institute of Experimental Physics, 040 01 Kosice, Slovakia*
- ¹³*Joint Institute for Nuclear Research, RU-141980 Dubna, Russia*
- ¹⁴*Duke University, Durham, North Carolina 27708, USA*
- ¹⁵*Fermi National Accelerator Laboratory, Batavia, Illinois 60510, USA*
- ¹⁶*University of Florida, Gainesville, Florida 32611, USA*
- ¹⁷*Laboratori Nazionali di Frascati, Istituto Nazionale
di Fisica Nucleare, I-00044 Frascati, Italy*
- ¹⁸*University of Geneva, CH-1211 Geneva 4, Switzerland*

City, IA 52242, USA, ⁿKinki University, Higashi-Osaka City, Japan 577-8502, ^oKansas State University, Manhattan, KS 66506, USA, ^pUniversity of Manchester, Manchester M13 9PL, United Kingdom, ^qQueen Mary, University of London, London, E1 4NS, United Kingdom, ^rUniversity of Melbourne, Victoria 3010, Australia, ^sMuons, Inc., Batavia, IL 60510, USA, ^tNagasaki Institute of Applied Science, Nagasaki, Japan, ^uNational Research Nuclear University, Moscow, Russia, ^vUniversity of Notre Dame, Notre Dame, IN 46556, USA, ^wUniversidad de Oviedo, E-33007 Oviedo, Spain, ^xTexas Tech University, Lubbock, TX 79609, USA, ^yUniversidad Tecnica Federico Santa Maria, 110v Valparaiso, Chile, ^zYarmouk University, Irbid 211-63, Jordan, ^{hh}On leave from J. Stefan Institute, Ljubljana, Slovenia,

- ¹⁹*Glasgow University, Glasgow G12 8QQ, United Kingdom*
- ²⁰*Harvard University, Cambridge, Massachusetts 02138, USA*
- ²¹*Division of High Energy Physics, Department of Physics, University of Helsinki and Helsinki Institute of Physics, FIN-00014, Helsinki, Finland*
- ²²*University of Illinois, Urbana, Illinois 61801, USA*
- ²³*The Johns Hopkins University, Baltimore, Maryland 21218, USA*
- ²⁴*Center for High Energy Physics: Kyungpook National University, Daegu 702-701, Korea; Seoul National University, Seoul 151-742, Korea; Sungkyunkwan University, Suwon 440-746, Korea; Korea Institute of Science and Technology Information, Daejeon 305-806, Korea; Chonnam National University, Gwangju 500-757, Korea; Chonbuk National University, Jeonju 561-756, Korea*
- ²⁵*Ernest Orlando Lawrence Berkeley National Laboratory, Berkeley, California 94720, USA*
- ²⁶*University of Liverpool, Liverpool L69 7ZE, United Kingdom*
- ²⁷*University College London, London WC1E 6BT, United Kingdom*
- ²⁸*Centro de Investigaciones Energeticas Medioambientales y Tecnologicas, E-28040 Madrid, Spain*
- ²⁹*Massachusetts Institute of Technology, Cambridge, Massachusetts 02139, USA*
- ³⁰*Institute of Particle Physics: McGill University, Montréal, Québec, Canada H3A 2T8; Simon Fraser University, Burnaby, British Columbia, Canada V5A 1S6; University of Toronto, Toronto, Ontario, Canada M5S 1A7; and TRIUMF, Vancouver, British Columbia, Canada V6T 2A3*
- ³¹*University of Michigan, Ann Arbor, Michigan 48109, USA*
- ³²*Michigan State University, East Lansing, Michigan 48824, USA*
- ³³*Institution for Theoretical and Experimental Physics, ITEP, Moscow 117259, Russia*
- ³⁴*University of New Mexico, Albuquerque, New Mexico 87131, USA*
- ³⁵*Northwestern University, Evanston, Illinois 60208, USA*
- ³⁶*The Ohio State University, Columbus, Ohio 43210, USA*
- ³⁷*Okayama University, Okayama 700-8530, Japan*
- ³⁸*Osaka City University, Osaka 588, Japan*

- ³⁹*University of Oxford, Oxford OX1 3RH, United Kingdom*
- ⁴⁰*Istituto Nazionale di Fisica Nucleare, Sezione di Padova-Trento,*
^{bb}*University of Padova, I-35131 Padova, Italy*
⁴¹*LPNHE, Universite Pierre et Marie*
Curie/IN2P3-CNRS, UMR7585, Paris, F-75252 France
- ⁴²*Istituto Nazionale di Fisica Nucleare Pisa,* ^{cc}*University of Pisa,*
^{dd}*University of Siena and* ^{ee}*Scuola Normale Superiore, I-56127 Pisa, Italy*
- ⁴³*University of Pittsburgh, Pittsburgh, Pennsylvania 15260, USA*
⁴⁴*Purdue University, West Lafayette, Indiana 47907, USA*
⁴⁵*University of Rochester, Rochester, New York 14627, USA*
⁴⁶*The Rockefeller University, New York, New York 10065, USA*
⁴⁷*Istituto Nazionale di Fisica Nucleare, Sezione di Roma 1,*
^{ff}*Sapienza Università di Roma, I-00185 Roma, Italy*
⁴⁸*Rutgers University, Piscataway, New Jersey 08855, USA*
⁴⁹*Texas A&M University, College Station, Texas 77843, USA*
⁵⁰*Istituto Nazionale di Fisica Nucleare Trieste/Udine,*
I-34100 Trieste, ^{gg}*University of Udine, I-33100 Udine, Italy*
⁵¹*University of Tsukuba, Tsukuba, Ibaraki 305, Japan*
⁵²*Tufts University, Medford, Massachusetts 02155, USA*
⁵³*University of Virginia, Charlottesville, Virginia 22906, USA*
⁵⁴*Waseda University, Tokyo 169, Japan*
⁵⁵*Wayne State University, Detroit, Michigan 48201, USA*
⁵⁶*University of Wisconsin, Madison, Wisconsin 53706, USA*
⁵⁷*Yale University, New Haven, Connecticut 06520, USA*

Abstract

We use a new method to estimate with 5% accuracy the contribution of pion and kaon in-flight-decays to the dimuon data set acquired with the CDF detector. Based on this improved estimate, we show that the total number and the properties of the collected dimuon events are not yet accounted for by ordinary sources of dimuons which also include the contributions, as measured in the data, of heavy flavor, Υ , and Drell-Yan production in addition to muons mimicked by hadronic punchthrough.

PACS numbers: 13.85.-t, 14.65.Fy, 13.20.Fc

I. INTRODUCTION

This article presents an improved determination of the composition of a dimuon sample recorded in $p\bar{p}$ collisions at $\sqrt{s} = 1.96$ TeV. The data sample consists of events containing two central ($|\eta| < 0.7$) primary (or trigger) muons, each with transverse momentum $p_T \geq 3$ GeV/ c , and with invariant mass larger than 5 GeV/ c^2 and smaller than 80 GeV/ c^2 . The sample may be dominated by real muon pairs due to semileptonic decays of heavy flavor, Drell-Yan production and Υ decays, but also contains events in which one or both muons are produced by hadrons that decay in flight or otherwise mimic a muon signal. Although the dimuon signature can be a powerful tool with which to search for new physics or sources of CP violation, the uncertainty of the in-flight-decay contribution makes the precise determination of the fractions of known processes a serious experimental challenge. In particular, it remains controversial if muons originating from the decay of objects with a lifetime longer than that of heavy-flavored hadrons can be completely accounted for with ordinary sources such as in-flight-decays. Earlier and recent studies estimate the fraction of this type of event to be negligible [1–3]. Other studies find it significant, suppress it by selecting muons produced close to the beamline [4], but have estimated its size with a very large uncertainty by using Monte Carlo simulations [5]. The present work is based on the same Monte Carlo simulated samples, and the same analysis methods as Refs. [4, 5], but we improve the method to estimate the number of events due to in-flight-decays achieving a 5% accuracy.

Section II describes the CDF II detector. In Sec. III, we review the present experimental situation. Sections IV to VI describe the procedure used to tune the simulation and estimate the contribution of ordinary sources to events in which muons are produced by objects with very long lifetimes. Based on this results, Section VII updates the estimate of the rate of multi-muon events reported in Ref. [5]. Our conclusions are presented in Sec VIII.

II. CDF II DETECTOR AND TRIGGER

CDF II is a multipurpose detector, equipped with a charged particle spectrometer and a finely segmented calorimeter. In this section, we describe the detector components that are relevant to this analysis. The description of these subsystems can be found in Refs. [6–15].

Two devices inside the 1.4 T solenoid are used for measuring the momentum of charged particles: the silicon vertex detector (SVXII and ISL) and the central tracking chamber (COT). The SVXII detector consists of microstrip sensors arranged in six cylindrical shells with radii between 1.5 and 10.6 cm, and with a total z coverage¹ of 90 cm. The first SVXII layer, also referred to as the L00 detector, is made of single-sided sensors mounted on the beryllium beam pipe. The remaining five SVXII layers are made of double-sided sensors and are divided into three contiguous five-layer sections along the beam direction z . The vertex z -distribution for $p\bar{p}$ collisions is approximately described by a Gaussian function with a rms of 28 cm. The transverse profile of the Tevatron beam is circular and has a rms spread of $\simeq 25 \mu\text{m}$ in the horizontal and vertical directions. The SVXII single-hit resolution is approximately $11 \mu\text{m}$ and allows a track impact parameter resolution of approximately $35 \mu\text{m}$, when also including the effect of the beam transverse size. The two additional silicon layers of the ISL help to link tracks in the COT to hits in the SVXII. The COT is a cylindrical drift chamber containing 96 sense wire layers grouped into eight alternating superlayers of axial and stereo wires. Its active volume covers $|z| \leq 155$ cm and 40 to 140 cm in radius. The transverse momentum resolution of tracks reconstructed using COT hits is $\sigma(p_T)/p_T^2 \simeq 0.0017 [\text{GeV}/c]^{-1}$. The trajectory of COT tracks is extrapolated into the SVXII detector, and tracks are refitted with additional silicon hits consistent with the track extrapolation.

The central muon detector (CMU) is located around the central electromagnetic and hadronic calorimeters, which have a thickness of 5.5 interaction lengths at normal incidence. The CMU detector covers a nominal pseudorapidity range $|\eta| \leq 0.63$ relative to the center of the detector, and is segmented into two barrels of 24 modules, each covering 15° in ϕ . Every module is further segmented into three submodules, each covering 4.2° in ϕ and consisting of four layers of drift chambers. The smallest drift unit, called a stack, covers a 1.2° angle in ϕ . Adjacent pairs of stacks are combined together into a tower. A track segment (hits in two out of four layers of a stack) detected in a tower is referred to as a

¹ In the CDF coordinate system, θ and ϕ are the polar and azimuthal angles of a track, respectively, defined with respect to the proton beam direction, z . The pseudorapidity η is defined as $-\ln \tan(\theta/2)$. The transverse momentum of a particle is $p_T = p \sin(\theta)$. The rapidity is defined as $y = 1/2 \cdot \ln((E + p_z)/(E - p_z))$, where E and p_z are the energy and longitudinal momentum of the particle associated with the track.

CMU stub. A second set of muon drift chambers (CMP) is located behind an additional steel absorber of 3.3 interaction lengths. The chambers are 640 cm long and are arranged axially to form a box around the central detector. The CMP detector covers a nominal pseudorapidity range $|\eta| \leq 0.54$ relative to the center of the detector. Muons which produce a stub in both the CMU and CMP systems are called CMUP muons. The CMX muon detector consists of eight drift chamber layers and scintillation counters positioned behind the hadron calorimeter. The CMX detector extends the muon coverage to $|\eta| \leq 1$ relative to the center of the detector.

The luminosity is measured using gaseous Cherenkov counters (CLC) that monitor the rate of inelastic $p\bar{p}$ collisions. The inelastic $p\bar{p}$ cross section at $\sqrt{s} = 1960$ GeV is scaled from measurements at $\sqrt{s} = 1800$ GeV using the calculations in Ref. [16]. The integrated luminosity is determined with a 6% systematic uncertainty [17].

CDF uses a three-level trigger system. At Level 1 (L1), data from every beam crossing are stored in a pipeline capable of buffering data from 42 beam crossings. The L1 trigger either rejects events or copies them into one of the four Level 2 (L2) buffers. Events that pass the L1 and L2 selection criteria are sent to the Level 3 (L3) trigger, a cluster of computers running speed-optimized reconstruction code.

For this study, we select events with two muon candidates identified by the L1 and L2 triggers. The L1 trigger uses tracks with $p_T \geq 1.5$ GeV/ c found by a fast track processor (XFT). The XFT examines COT hits from the four axial superlayers and provides $r - \phi$ information in azimuthal sections of 1.25° . The XFT passes the track information to a set of extrapolation units that determine the CMU towers in which a CMU stub should be found if the track is a muon. If a stub is found, a L1 CMU primitive is generated. The L1 dimuon trigger requires at least two CMU primitives, separated by at least two CMU towers. The L2 trigger additionally requires that at least one of the muons also has a CMP stub matched to an XFT track with $p_T \geq 3$ GeV/ c . All these trigger requirements are emulated by the detector simulation on a run-by-run basis. The L3 trigger requires a pair of CMUP muons with invariant mass larger than 5 GeV/ c^2 , and $|\delta z_0| \leq 5$ cm, where z_0 is the z coordinate of the muon track at its point of closest approach to the beamline in the $r - \phi$ plane. These requirements define the dimuon trigger used in this analysis.

III. PRESENT UNDERSTANDING OF THE DIMUON SAMPLE COMPOSITION

The value of $\sigma_{b \rightarrow \mu, \bar{b} \rightarrow \mu}$ and $\sigma_{c \rightarrow \mu, \bar{c} \rightarrow \mu}$, the correlated cross sections for producing pairs of central heavy-flavored quarks that decay semileptonically, is derived in Ref. [4] by fitting the impact parameter [18] distribution of the primary muons with the expected shapes from all sources believed to be significant: semileptonic heavy flavor decays, prompt quarkonia decays, Drell-Yan production, and instrumental backgrounds due to punchthrough of prompt or heavy-flavored hadrons which mimic a muon signal [19]. In the following, the sum of these processes will be referred to as the prompt plus heavy flavor ($P + HF$) contribution. The notation $K^{puth} \rightarrow \mu$ and $\pi^{puth} \rightarrow \mu$ will be used to indicate muon signals mimicked by punchthrough of kaons and pions, respectively. In order to properly model the data with the templates of the various $P + HF$ sources, the study in Ref. [4] has used strict selection criteria, referred to as tight SVX selection in the following, by requiring muon tracks with hits in the two innermost layers of the SVX detector, and in at least two of the next four outer layers.

The tight SVX requirements select events in which both muons arise from parent particles that have decayed within a distance of $\simeq 1.5$ cm from the $p\bar{p}$ interaction primary vertex in the plane transverse to the beamline. This requirement suppresses the yield of primary muons due to in-flight-decays of pions and kaons, in the following referred to as $\pi^{ifd} \rightarrow \mu$ and $K^{ifd} \rightarrow \mu$, respectively. This type of contribution to the dimuon dataset prior to any SVX requirement was considered negligible in previous [1, 2] and recent [3] studies by the CDF and D0 collaborations.

As shown by Fig. 1, the tight SVX sample is well modeled by fits using the prompt and heavy flavor contributions [4]. The sample composition determined by the fit and corrected for the appropriate efficiency of the tight SVX requirements ² is listed in the first two columns of Table I.

The difference between the total number of dimuons and the $P + HF$ component indicates the presence of an important source of dimuons produced beyond 1.5 cm which is suppressed

² The efficiency of the tight SVX selection has been measured [5] to be 0.257 ± 0.004 for prompt dimuons and 0.237 ± 0.001 for dimuons produced by heavy flavor decays by using control samples of data from various sources ($J/\psi \rightarrow \mu^+ \mu^-$, $B^\pm \rightarrow \mu^+ \mu^- K^\pm$, $B \rightarrow \mu D^0$, and $\Upsilon \rightarrow \mu^+ \mu^-$).

TABLE I: Number of events attributed to the different dimuon sources by the fit to the muon impact-parameter distribution. The fit parameters BB , CC , and PP represent the $b\bar{b}$, $c\bar{c}$, and prompt dimuon contributions, respectively. The component BC represents events containing b and c quarks. The fit parameter BP (CP) estimates the number of events in which there is only one b (c) quark in the detector acceptance and the second muon is produced by prompt hadrons in the recoiling jet that mimic a muon signal. Real muons are muons from semileptonic decay of heavy flavors, Drell-Yan production or quarkonia decays. The data correspond to an integrated luminosity of 742 pb^{-1} . The dimuon data set consists of 743006 events.

Component	No. of Events	No. of real $\mu - \mu$	No. and type of misidentified μ
BB	230308 ± 2861	$R_{bb} \times BB$	$R_{bb} \times [7902 K^{p\text{uth}} \rightarrow \mu$ $+ 8145 \pi^{p\text{uth}} \rightarrow \mu]$
CC	103198 ± 6603	$R_{cc} \times CC$	$R_{cc} \times [17546 K^{p\text{uth}} \rightarrow \mu$ $+ 9535 \pi^{p\text{uth}} \rightarrow \mu]$
PP	161696 ± 2533	$\Upsilon = 51680 \pm 649$ $+ DY = 54200 \pm 5420$	$4400 K^{p\text{uth}} \rightarrow \mu K^{p\text{uth}} \rightarrow \mu$ $+ 30000 \pi^{p\text{uth}} \rightarrow \mu \pi^{p\text{uth}} \rightarrow \mu$ $+ 23000 K^{p\text{uth}} \rightarrow \mu \pi^{p\text{uth}} \rightarrow \mu$
BP	43096 ± 3087		$11909 K^{p\text{uth}} \rightarrow \mu + 29253 \pi^{p\text{uth}} \rightarrow \mu$
CP	41582 ± 5427		$16447 K^{p\text{uth}} \rightarrow \mu + 35275 \pi^{p\text{uth}} \rightarrow \mu$
BC	9135 ± 2924		
$P + HF$	589015 ± 5074		

by the tight SVX requirements. Because unnoticed by previous experiments, this source was whimsically referred to as the ghost contribution.

The relative size of the ghost and $P + HF$ contributions depends upon the type of SVX requirement applied to the trigger muons. Reference [5] shows that neglecting the presence of ghost events affected previous measurements of $\sigma_{b \rightarrow \mu, \bar{b} \rightarrow \mu}$ [1, 20] and of $\bar{\chi}$ [2] at the Tevatron. Finally, the ghost sample is shown to be the source of the dimuon invariant mass discrepancy observed in Ref. [21].

Reference [5] has studied a number of potential sources of muons originating beyond

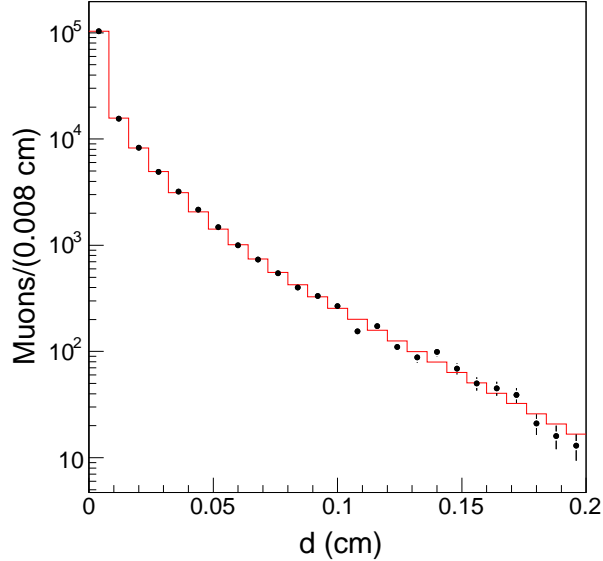


FIG. 1: The projection of the two-dimensional impact parameter distribution of muon pairs onto one of the two axes is compared to the fit result (histogram).

the beam pipe. Contrary to what assumed by previous experiments, the one source found to contribute significantly arises from in-flight-decays of pions and kaons. Based upon a generic QCD simulation, that study estimates a contribution of 57000 events. A smaller contribution (12052 ± 466 events) from K_S^0 and hyperon decays in which the punchthrough of a hadronic prong mimics a muon signal was estimated using the data. Secondary inelastic interactions in the tracking volume were found to be a negligible source of ghost events. The final estimate of the size of possible sources of ghost events underpredicts the observed number by approximately a factor of two (154000 observed and 69000 accounted for), but the difference was not considered significant because of the simulation uncertainty.

The present study uses events selected with the tight SVX requirements to tune the QCD simulation. Since these data are well modeled by the impact parameter templates of the $P + HF$ components, misidentified muons can only arise from the punchthrough of prompt hadrons or hadrons produced by heavy-flavor decays. The numbers of misidentified muons in the data are derived by subtracting the expected number of real muons, listed in the third column of Table I, from the corresponding components in the second column. We then compare these differences to the rate of $K^{puth} \rightarrow \mu$ and $\pi^{puth} \rightarrow \mu$ misidentifications predicted by the simulation, and listed on the fourth column of the same table. The simulation is

tuned by adjusting the predicted rate of pions and kaons to reproduce the observed number of muon misidentifications. Then, the tuned simulation is used to predict the number of muons due to in-flight-decays with 5% accuracy.

IV. RATES OF MISIDENTIFIED MUONS IN THE DATA AND SIMULATION

We make use of three different samples of simulated events generated with the HERWIG parton-shower Monte-Carlo program [22], the settings of which are described in Appendix A of Ref. [4]. We use option 1500 of the HERWIG program to generate final states produced by hard scattering of partons with transverse momentum larger than 3 GeV/ c (sample A=generic QCD). Hadrons with heavy flavors are subsequently decayed using the EVTGEN Monte Carlo program [23]. The detector response to particles produced by the above generators is modeled with the CDF II detector simulation that in turn is based on the GEANT Monte Carlo program [24]. The values of the heavy flavor cross sections predicted by the generator are scaled to the measured values $\sigma_{b \rightarrow \mu, \bar{b} \rightarrow \mu} = 1549 \pm 133$ pb and $\sigma_{c \rightarrow \mu, \bar{c} \rightarrow \mu} = 624 \pm 104$ pb [4]. The next simulated sample (sample B=single b + single c) is extracted from A by requiring the presence of at least a trigger muon generated from heavy-flavor semileptonic decays. The simulated sample C= $b\bar{b}$ + $c\bar{c}$ is extracted from B by requiring the presence of at least two trigger muons generated from heavy flavor decays. This sample has been used to construct impact parameter templates and estimate kinematic acceptances in Ref. [4].

In the various simulations, we evaluate the number of dimuons from heavy flavor decays and the number of pairs of tracks of different type that pass the same kinematic selection. The ratios of these numbers are listed in Tables II to IV. The rate of pairs of tracks of different type predicted by the simulation are normalized to the data by multiplying these ratios by the number of dimuons from $b\bar{b}$ or $c\bar{c}$ production observed in the data.

TABLE II: Ratio of the numbers of $\pi\pi$, KK , and $K\pi$ pairs to that of primary dimuons from $b\bar{b}$ decays (221096 pairs) in the generic QCD simulation (sample A).

Process	R_{KK}	$R_{K\pi}$	$R_{\pi\pi}$
generic QCD	867	8935	22913

TABLE III: Ratio of the numbers of $\mu - K(\pi)$ combinations to that of primary dimuons from $b\bar{b}$ and $c\bar{c}$ production in the single- b and single- c simulated samples (221096 and 83590 dimuons, respectively).

Process	R_K	R_π
single b	11.1	54.4
single c	40.7	173.7

TABLE IV: Ratio of the numbers of $\mu - K(\pi)$ combinations to that of primary dimuons from heavy flavor production in the $b\bar{b}$ and $c\bar{c}$ simulated samples (221096 and 83590 dimuons, respectively).

Process	R_K	R_π
$b\bar{b}$	7.4	15.2
$c\bar{c}$	43.5	46.9

The probability $P_{K(\pi)}^{puth}$ that a kaon (pion) is not contained by the calorimeter and mimics a muon signal has been measured in Ref. [4] by using kaons and pions from $D^{*\pm} \rightarrow \pi^\pm D^0$ with $D^0 \rightarrow K^+ \pi^-$ decays. The probability that kaon (pion) in-flight-decays mimic a trigger muon, $P_{K(\pi)}^{ifd}$, has been derived in Ref. [5] by using the simulated sample C. These probabilities depend on the particle transverse momentum. Table V lists the average probabilities that kaons (pions) mimic a primary muon when applying the $P_{K(\pi)}^{puth}$ and $P_{K(\pi)}^{ifd}$ probabilities to simulated kaon (pion) tracks with $p_T \geq 3$ GeV/ c and $|\eta| < 0.7$.

TABLE V: Average probabilities (%) that punchthroughs or in-flight decays result into a primary muon. The p_T distribution of kaons and pions in the different simulations are almost indistinguishable.

$\langle P_K^{puth} \rangle$	$\langle P_\pi^{puth} \rangle$	$\langle P_K^{ifd} \rangle$	$\langle P_\pi^{ifd} \rangle$
0.483 ± 0.003	0.243 ± 0.004	0.345 ± 0.005	0.0727 ± 0.0016

By weighting simulated pion (kaon) tracks that pass the muon kinematic selection with

the corresponding $P_{K(\pi)}^{puth}$ probability, we obtain the prediction of misidentified primary muons for the various $P + HF$ components that is listed in the fourth column of Table I. The third column of the same table lists the number of real muons for the various $P + HF$ contributions. The sum of real plus misidentified muon pairs is in general agreement with the data listed in the second column of the table. Therefore, it is reasonable to use the observed rate of dimuons, the knowledge of the fraction of real dimuons due to semileptonic decay of heavy flavors, Drell-Yan or Υ mesons, and the knowledge of the $P_{K(\pi)}^{puth}$ probabilities to normalize the absolute yields of pions and kaons predicted by the simulation. The simulation fitted to the data is then used to predict the rate of events due to in-flight-decay misidentifications by weighting simulated tracks with the $P_{K(\pi)}^{ifd}$ probabilities, the average of which is listed in Table V. In addition, the total rate of $K \rightarrow \mu = K^{puth} \rightarrow \mu + K^{ifd} \rightarrow \mu$ misidentifications predicted by the simulation can be further constrained with data. This is done in the next section by using the number of primary muons due to misidentification of K^{*0} , $K^{*\pm}$, and K_S^0 decays.

We first describe the evaluation of the content of real muons in the various $P + HF$ components and the function used to fit the simulation to the data. Reference [4] estimates that the fraction $R_{bb} = 0.96 \pm 0.04$ of the BB component is due to real muons from b -quark semileptonic decays whereas the remaining 4% is due to muons mimicked by the punchthrough of hadrons produced by heavy flavor decays. Similarly, the fraction $R_{cc} = 0.81 \pm 0.09$ of the CC component is due to real muons from c -quark semileptonic decays whereas the remaining 19% is due to muons mimicked by the punchthrough of hadrons produced by heavy flavor decays. The uncertainty of the fraction of real muons due to $b\bar{b}$ ($c\bar{c}$) production is accounted for by multiplying R_{bb} (R_{cc}) by the fit parameter f_{bb} (f_{cc}) constrained to 1 with a 4% (11%) Gaussian error.

The number of Υ mesons contributing to the PP component ($\Upsilon = 51680 \pm 649$ candidates) has been determined in Ref. [4] by fitting the dimuon invariant mass spectrum with three Gaussian functions to model the signal and a straight line to model the combinatorial background. The Drell-Yan contribution is evaluated as $DY = \Upsilon \times \sigma_{DY}/\sigma_{\Upsilon}$. The cross section σ_{DY} in the $5 - 80 \text{ GeV}/c^2$ mass range is evaluated with a NLO calculation [25], and we use the measured value of σ_{Υ} [26]. The ratio $\sigma_{DY}/\sigma_{\Upsilon}$ is 1.05 with a 10% error mostly due to the measurement in Ref. [26]. To account for the uncertainty, we weight the DY contribution with the fit parameter f_{dy} constrained to 1 with a 10% Gaussian error.

The magnitude of the BP (CP) component, predicted with the single- b (single- c) simulation, with respect to that of the BB (CC) contribution depends on the ratio of NLO to LO terms evaluated by the HERWIG generator. Because of the dependence on the renormalization and factorization scales, the uncertainty of the single- b (c) cross section to that of the $b\bar{b}$ ($c\bar{c}$) cross section is estimated [27] to be $\simeq 20$ (30)%³. We account for this uncertainty by weighting the rate of pion and kaon tracks predicted by the single- b (single- c) simulation with the additional fit parameter f_{sb} (f_{sc}) constrained to 1 with a 20% (30%) Gaussian error.

The simulation prediction of the number of muons mimicked by the punchthrough of pions (kaons) is weighted with the fit free parameter f_π (f_K). These fit parameters provide the absolute normalization of the pion (kaon) rate predicted by the simulation including the uncertainties of the punchthrough probabilities.

V. MEASUREMENT OF THE $K \rightarrow \mu$ CONTRIBUTION

The small rate of $K \rightarrow \mu = K^{puth} \rightarrow \mu + K^{ifd} \rightarrow \mu$ misidentifications is measured using a higher statistics sample of dimuon events corresponding to an integrated luminosity of 3.9 fb⁻¹. The number of $K \rightarrow \mu$ misidentification, N_K , is derived from $N_{K^{*0}}$, the number of identified $K^{*0} \rightarrow K^+\pi^-$ decays with $K^+ \rightarrow \mu^+$ (and charge-conjugate states). The number $N_{K^{*0}}$ is related to N_K by

$$N_{K^{*0}} = N_K \cdot \epsilon_0 \cdot R(K^{*0}),$$

where $R(K^{*0})$ is the fraction of kaons that result from $K^{*0} \rightarrow K^+\pi^-$ decays and ϵ_0 is the efficiency to reconstruct the pion.

We also select $K_S^0 \rightarrow \pi^+\pi^-$ with $\pi \rightarrow \mu$ candidates and reconstruct $K^{*\pm} \rightarrow K_S^0\pi^\pm$ decays. The number of $K^{*\pm}$ is related to that of K_S^0 by

$$N_{K^{*\pm}} = N_{K_S^0} \cdot \epsilon_1 \cdot R(K^{*\pm}),$$

where $R(K^{*\pm})$ is the fraction of K_S^0 resulting from $K^{*\pm} \rightarrow K_S^0\pi^\pm$ decays and ϵ_1 is the efficiency to reconstruct the additional pion. We use isospin invariance to set $R(K^{*\pm}) = R(K^{*0})$. Since the additional pion used to search for the $K^{*\pm}$ and K^{*0} candidates is selected

³ However, the study in Ref. [28] shows that the HERWIG generator predicts the observed single and correlated heavy-flavor cross sections to better than 10%.

with the same kinematic requirements, we set $\epsilon_0 = \epsilon_1$. It follows that

$$N_K = N_{K_S^0}/N_{K^{*\pm}} \times N_{K^{*0}}.$$

We search for K^{*0} decays by combining primary muons, assumed to be kaons, with all opposite charge tracks, assumed to be pions, with $p_T \geq 0.5$ GeV/ c and in an angular cone with $\cos \theta \geq 0.6$ around the direction of the primary muon. We require tracks with at least 10 axial and 10 stereo COT hits. We constrain the pair to arise from a common three-dimensional point, and reject combinations if the probability of the vertex-constrained fit is smaller than 0.001. The invariant mass spectrum of the selected $K^{*0} \rightarrow K^+\pi^-$ candidates is shown in Fig. 2. We fit the invariant mass distribution with a Breit-Wigner function

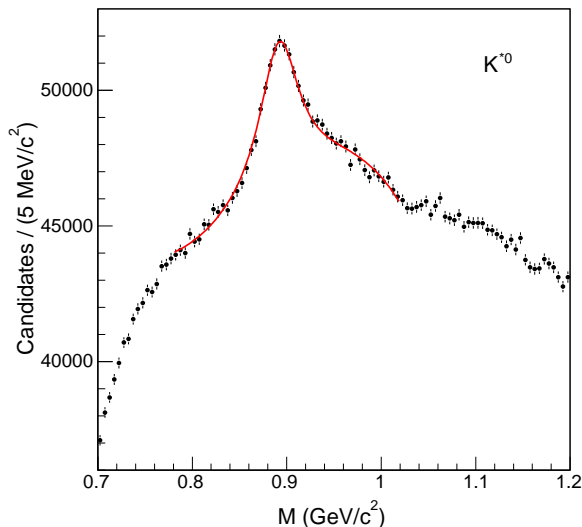


FIG. 2: Invariant mass distribution of $K^{*0} \rightarrow K^+\pi^-$ candidates passing our selection criteria. The line represents the fit described in the text.

smearred by the detector mass resolution to model the signal. We fix the mass and width of the Breit-Wigner function to 896 and 51 MeV/ c^2 [29], respectively ⁴. We use a fourth order polynomial to model the combinatorial background under the signal, and the fitted range of invariant mass is conveniently chosen to yield a fit with 50% probability. The size of the signal is not affected by the arbitrary choice of the function used to model the combinatorial

⁴ The mass resolution due to the track reconstruction in simulated events which include kaon in-flight-decays is 4.9 MeV/ c^2 , and is negligible compared to the resonance width.

background or of the fitted mass range, and is solely determined by the accurate knowledge of the signal shape. The fit yields $N_{K^{*0}} = 87471 \pm 2217 K^{*0}$ mesons.

We search for $K_S^0 \rightarrow \pi^+\pi^-$ with a $\pi \rightarrow \mu$ misidentification by combining primary muons with tracks passing the same requirements as those used in the K^{*0} search. In this case, both tracks are assumed to be pions. As in the previous case, we select pairs consistent with arising from a common three-dimensional vertex. We take advantage of the K_S^0 long lifetime to suppress the combinatorial background. We further require that the distance between the K_S^0 vertex and the event primary vertex, corrected by the K_S^0 Lorentz boost, corresponds to $ct > 0.1$ cm. The invariant mass of the K_S^0 candidates is shown in Fig. 3.

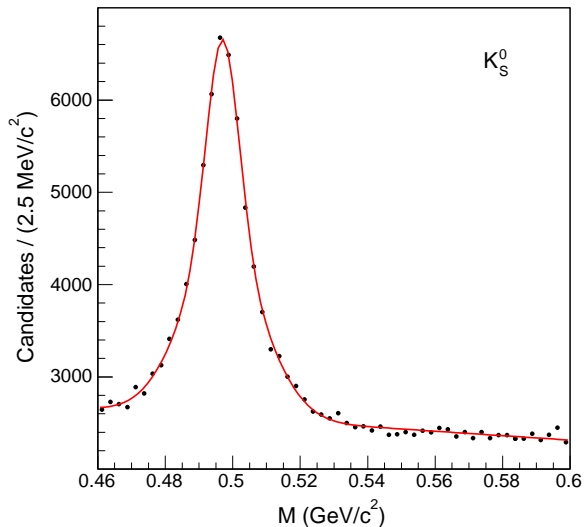


FIG. 3: Invariant mass distribution of K_S^0 candidates passing our selection criteria. The line represents the fit described in the text.

We fit the signal with two Gaussian functions and the combinatorial background with a straight line in the mass range $0.4 - 0.6 \text{ GeV}/c^2$. Having fixed the peak of the Gaussian functions at $0.497 \text{ GeV}/c^2$ [29], the fit returns an averaged σ of $8.4 \text{ MeV}/c^2$, consistent with what is expected from simulated events ⁵, and a signal of $32445 \pm 421 K_S^0$ mesons in the mass range $0.474 - 0.522 \text{ GeV}/c^2$.

⁵ Because of the K_S^0 long decay path, reconstructed track segments may be shorter than the available tracking detector length. When K_S^0 mesons decay before entering the COT volume, the mass resolution is $4 \text{ MeV}/c^2$.

We search for $K^{*\pm}$ by combining K_S^0 candidates with mass between 0.474 and 0.522 GeV/c^2 and $ct > 0.1$ cm with any additional track, assumed to be a pion, that pass the same selection as pion tracks used to find K^{*0} candidates. We constrain the K_S^0 mass to 0.497 GeV/c^2 and require that the K_S^0 candidate and the pion track are consistent with arising from a common three-dimensional vertex. The invariant mass distribution of $K^{*\pm}$ candidates is shown in Fig. 4.

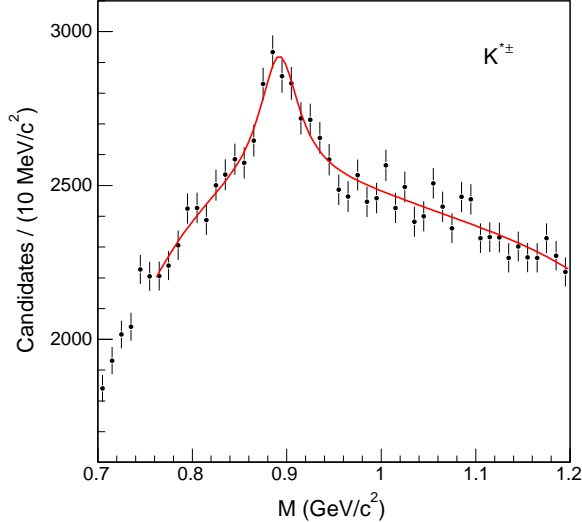


FIG. 4: Invariant mass distribution of $K^{*\pm} \rightarrow K_S^0 \pi^\pm$ candidates passing our selection criteria. The line represents the fit described in the text.

We fit the invariant mass distribution with a Breit-Wigner function to model the signal and a fourth order polynomial to model the combinatorial background. We fix the mass and width of the Breit-Wigner function to 892 and 51 MeV/c^2 [29], respectively ⁶. The fit returns a signal of 3326 ± 246 $K^{*\pm}$ mesons.

The signals obtained by analyzing the 3.9 fb^{-1} sample are rescaled to estimate the number of $K \rightarrow \mu$ misidentifications present in the 742 pb^{-1} dataset. After rescaling, we obtain $N_K = N_{K_S^0}/N_{K^{*\pm}} \times N_{K^{*0}} = 164769 \pm 13067$. This number is used to constrain the total number N_K^{sim} of $K \rightarrow \mu$ misidentifications predicted by the simulation.

⁶ In simulated events, when constraining the K_S^0 mass to the PDG value, the mass-constrained K_S^0 momentum is measured as accurately as that of a track corresponding to a $K \rightarrow \mu$ decay. The resulting $K^{*\pm}$ mass resolution is approximately 5 MeV/c^2 .

VI. FIT OF THE SIMULATION PREDICTION TO THE DATA

We fit the simulation prediction with a χ^2 -minimization method [30]. The χ^2 function is defined as

$$\chi^2 = \sum_{i=1}^5 (D[i] - P[i])^2 / ED[i]^2 + (N_K^{\text{sim}} - 164769)^2 / 13067^2 ,$$

where $D[i]$ and $ED[i]$ are the size and error of the component listed in the second column and i -th row of Table I. The term $P[i]$ is the sum of the real muon contribution and the punchthrough contribution predicted by the simulation in the third and fourth columns of the same table, respectively. These contributions are weighted with the fit parameters described in the previous section, and the terms read

$$P[1] = f_{bb} (0.96 \cdot 230308 + f_k 7902 + f_\pi 8145),$$

$$P[2] = f_{cc} (0.81 \cdot 103198 + f_k 17546 + f_\pi 9535),$$

$$P[3] = \Upsilon + f_{dy} DY + f_K^2 4400 + f_\pi^2 30000 + f_K f_\pi 23000,$$

$$P[4] = f_{sb} (f_K 11909 + f_\pi 29253), \text{ and}$$

$$P[5] = f_{sc} (f_K 16447 + f_\pi 35275).$$

In addition, the sum $\sum_{i=1}^5 D[i]$ is constrained to the observed number of $P + HF - BC$ events within its error. The fit results are shown in Tables VI to VIII. In Table VI, the fit parameters that tune the various cross sections predicted by the HERWIG generator are very close to their nominal values indicating that the default simulation provides a quite accurate modeling of the data.

The fit returns 163501 $K \rightarrow \mu$ candidates (164769 ± 13067 are measured in the data), 51% of which are due to punchthrough and 49% to in-flight-decays. We verify this result by measuring the fraction of $K \rightarrow \mu$ decays in identified $K^{*0} \rightarrow K^+\pi^-$ decays that pass the tight SVX requirements. The efficiencies of the tight SVX requirement applied to primary muons are 0.356 ± 0.002 for muons due to punchthrough of prompt and heavy-flavored hadrons and 0.166 ± 0.005 for muons arising from in-flight decays ⁷. Based on the kaon composition

⁷ In Ref. [5], which uses 0.74 fb^{-1} of data, these efficiencies have been measured to be 0.45 and 0.21, respectively. In 3.9 fb^{-1} of data, by using Υ candidates, we measure a smaller efficiency of the tight SVX selection. The efficiency loss comes from periods of data taking in which the pedestals of the L00 channels were miscalibrated.

TABLE VI: Parameter values returned by the fit described in the text. The fit yields $\chi^2 = 2.5$ for 5 DOF.

f_{bb}	0.97 ± 0.01
f_{cc}	0.95 ± 0.04
f_{dy}	1.01 ± 0.09
f_{π}	0.97 ± 0.08
f_K	1.01 ± 0.08
f_{sb}	1.05 ± 0.08
f_{sc}	0.82 ± 0.10

TABLE VII: Parameter correlation coefficients returned by the fit.

Fit parameter	f_{bb}	f_{cc}	f_{dy}	f_{π}	f_K	f_{sb}
f_{cc}	-0.11					
f_{dy}	0.17	0.10				
f_{π}	-0.16	-0.10	-0.84			
f_K	-0.08	-0.17	0.71	-0.48		
f_{sb}	-0.07	-0.03	0.50	-0.51	-0.01	
f_{sc}	-0.02	-0.21	0.36	-0.35	-0.12	0.15

returned by the fit, we estimate the efficiency of the tight SVX requirement applied to $K \rightarrow \mu$ misidentifications to be 0.263 ± 0.008 , where the error includes the uncertainty of the efficiencies and that of the kaon composition returned by the fit. Figure 5 shows the invariant mass distribution of K^{*0} candidates after applying the tight SVX requirement. We fit the invariant mass distribution with the same function used to fit the K^{*0} mass distribution in Fig. 2. The fit returns 22689 ± 985 K^{*0} candidates to be compared with 87741 ± 2219 K^{*0} candidates before applying the tight SVX requirement. The resulting efficiency of the tight SVX requirement is 0.253 ± 0.013 , in agreement with what expected (0.263 ± 0.008) using the composition of the kaon sample returned by the fit.

TABLE VIII: Number of events due to different production mechanisms are compared to the result of the present fit.

Component	No. of Events	Fit result
BB	230308 ± 2861	230607
CC	103198 ± 6603	104463
PP	161696 ± 2533	161387
BP	43096 ± 3087	42490
CP	41582 ± 5427	41822
$P + HF$	589015 ± 5074	589905

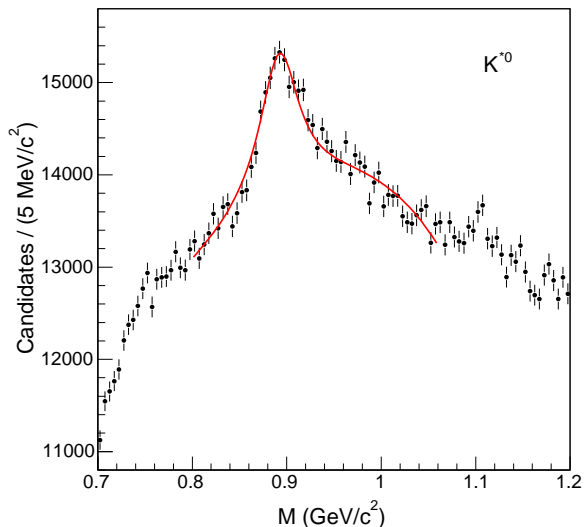


FIG. 5: Invariant mass distribution of K^{*0} candidates in which the $K \rightarrow \mu$ misidentification passes the tight SVX requirement. The line represents the fit described in the text.

Continuing with the analysis of the results returned by the fit, the total number of $\pi \rightarrow \mu$ misidentifications is 240915, 64% of which are due to punchthrough and 36% to in-flight-decays. The fractional composition of the $K \rightarrow \mu$ and $\pi \rightarrow \mu$ misidentifications is summarized in Table IX.

The total fraction of misidentified muons in the dataset is 27%. The number of misidentified muons due in-flight-decays of pions and kaons (ghost events) is 113613 ± 5332 . Since the

TABLE IX: Contributions (%) of various processes to pion or kaon misidentifications.

Type	$K^{puth} \rightarrow \mu$	$\pi^{puth} \rightarrow \mu$
All sample	51	64
generic QCD	20	33
single $b + b\bar{b} +$		
single $c + c\bar{c}$	31	31
Type	$K^{ifd} \rightarrow \mu$	$\pi^{ifd} \rightarrow \mu$
All sample	49	36
generic QCD	27	27
single $b + b\bar{b} +$		
single $c + c\bar{c}$	22	9

number of muons from in-flight-decays is derived from that of muons mimicked by hadron punchthrough using the fake probabilities listed in Table V, the uncertainty of these probabilities yields an additional error of 3845 events.

After adding the 12052 ± 466 events from K_S^0 and hyperon decays, we predict 125665 ± 5351 ghost events, whereas the dimuon dataset contains 153991 ± 5074 events of this type. The number of unaccounted events (28326 ± 7374) is $(12.8 \pm 3.2)\%$ of the $b\bar{b}$ production and $(18.3 \pm 4.7)\%$ of the ghost sample.

VII. REVISED ESTIMATE OF THE RATE OF ADDITIONAL REAL MUONS IN GHOST EVENTS

As a cross-check of its $b\bar{b}$ content, Reference [5] has investigated the rate of sequential semileptonic decays of single b quarks in the dimuon sample. We provide here a summary of that study and its conclusions. That study searches for additional muons with $p_T \geq 2 \text{ GeV}/c$ and $|\eta| \leq 1.1$ in a dimuon sample corresponding to an integrated luminosity of 1426 pb^{-1} . The sample of 1426571 events contains 1131090 ± 9271 $P + HF$ events in which both muons originate inside the beam pipe and 295481 ± 9271 ghost events in which at least one muon is produced outside. The study selects pairs of primary and additional muons with opposite

charge (OS) and invariant mass smaller than $5 \text{ GeV}/c^2$.

In the case of Drell-Yan or quarkonia production, which was not simulated, the rate of same-charge pairs (SS) is a measure of the fake muon contribution since misidentified muons arise from the underlying event which has no charge correlation with primary muons. The rate of additional muons mimicked by hadronic punchthrough is also estimated with a probability per track derived by using kaons and pions from $D^{*\pm} \rightarrow \pi^\pm D^0$ with $D^0 \rightarrow K^+\pi^-$ decays. This misidentification probability is approximately ten times larger than that for primary muons that have to penetrate twice as many interaction lengths⁸. The punchthrough probabilities for pions and kaons differ by a factor of two. In addition, in simulated events due to heavy flavor production, the pion to kaon ratio depends on the invariant mass and the charge of the muon-hadron pairs. Therefore, for $P + HF$ events, the rate of $OS - SS$ pairs is compared to that predicted by the heavy flavor simulation in which pions and kaons are weighted with the corresponding probabilities of mimicking a muon signal. In $P + HF$ events, the number of sequential semileptonic decay-candidates (29262 ± 850) is correctly modeled by the rate of sequential decays of single b -quarks predicted by the simulation (29190 ± 1236). This number is 2.5% of the $P + HF$ total contribution and $(6.9 \pm 0.4)\%$ of the $b\bar{b}$ contribution (424506 ± 18454 events).

In the remaining 295481 ± 9271 ghost events, the number of additional muons in an angular cone with $\cos\theta \geq 0.8$ around a primary muon is 49142 ± 519 . In the absence of a simulation of ghost events, that study assumes that tracks in ghost events are a 50-50% mixture of pion and kaons, and estimates the number of misidentified additional muons to be 20902 ± 284 . The resulting number of unaccounted ghost events with three or more muons is 27970 ± 538 , $(9.5 \pm 0.4)\%$ of the ghost events.

As shown by Table IX, one half of the ghost events arise from heavy flavor production acquired with a misidentified muon. This type of event should contain an appreciable fraction of additional muons due to semileptonic decays of heavy quarks. This contribution was not included in the estimate of Ref. [5].

We estimate this contribution using K_S^0 and K^{*0} candidates due to $\pi \rightarrow \mu$ and $K \rightarrow \mu$ misidentification, respectively. As shown in Sec. V, there are 32445 ± 421 and 87471 ± 2217

⁸ Therefore, the contribution of in-flight-decays to additional muons is negligible in comparison with the punchthrough contribution.

candidates, respectively. We measure the fraction of these candidates in which at least one of the primary muons is accompanied by an additional muon in a $\cos\theta \geq 0.8$ angular cone around its direction. We also estimate the contribution of fake additional muon by weighting all hadronic tracks that pass the additional muon selection criteria, assumed to be a 50-50% mixture of pions and kaons, with the corresponding misidentification probabilities [5].

Figure 6 (7) shows the invariant mass distribution of K_S^0 (K^{*0}) candidates when at least one primary muon is accompanied by an additional muon or a predicted misidentified muon.

As previously done, we fit the K_S^0 distributions with two Gaussian functions to model the

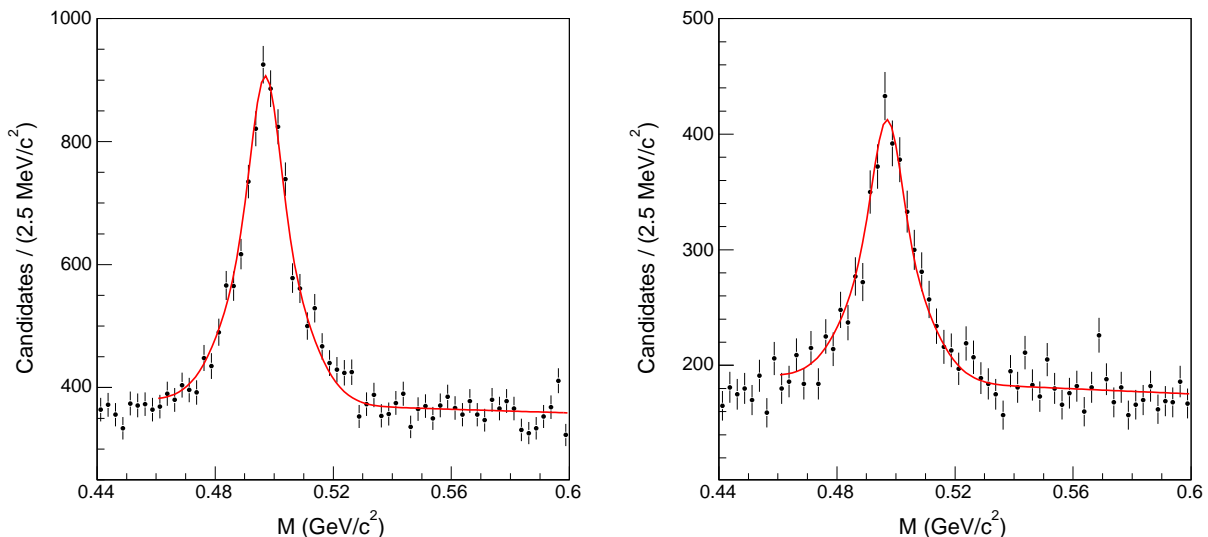


FIG. 6: Invariant mass distribution of K_S^0 candidates accompanied by (left) an additional muon and (right) a misidentified muon. Lines represent the fits described in the text.

signal and a straight line to model the background. The K^{*0} distribution is fitted with a Breit-Wigner function plus a fourth order polynomial.

The fits return 4572 ± 91 and 1954 ± 109 events in which a K_S^0 meson is accompanied by an additional muon and by a fake muon, respectively. The fits return 10176 ± 739 and 5230 ± 493 events in which a K^{*0} meson is accompanied by an additional muon and by a fake muon, respectively.

As shown in Fig. 8 for events triggered by K_S^0 misidentifications, sometimes the additional muon is contributed by the second prong of the K_S^0 decay. Figure 8 shows the invariant mass distribution of primary and additional muons that pass the analysis selection. The usual fit

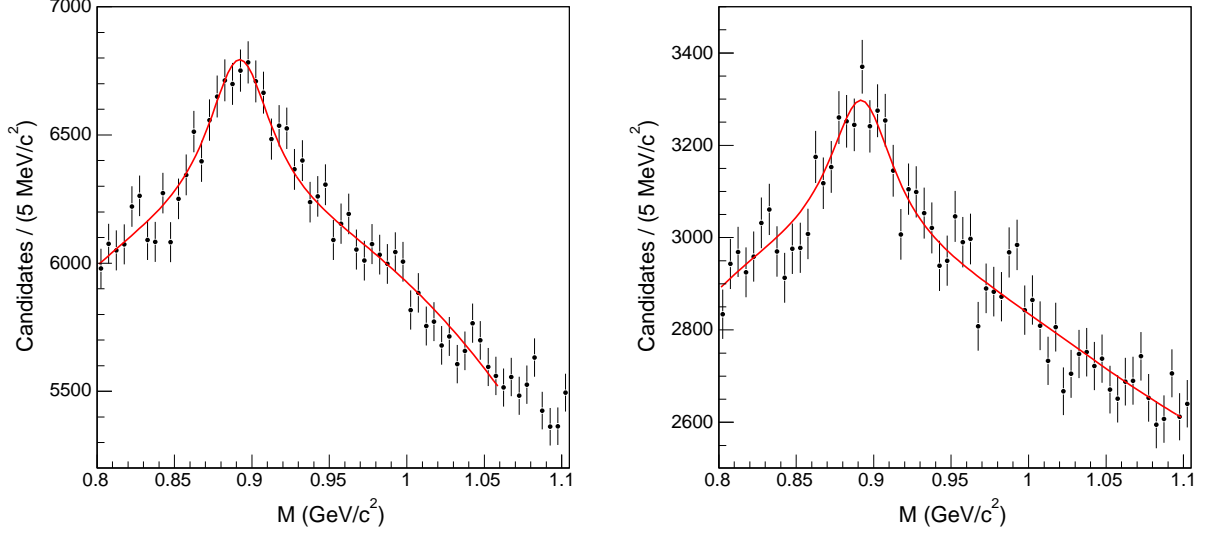


FIG. 7: Invariant mass distribution of K^{*0} candidates accompanied by (left) an additional muon and (right) a misidentified muon. Lines represent the fits described in the text.

yields 403 ± 33 events in which the additional muon is mimicked by the second leg of the K_S^0 decay that also produced the primary muon. We remove this contribution to evaluate the fraction of real muons accompanying $K \rightarrow \mu$ misidentifications. We will add it for the fraction of events triggered by misidentified K_S^0 decays.

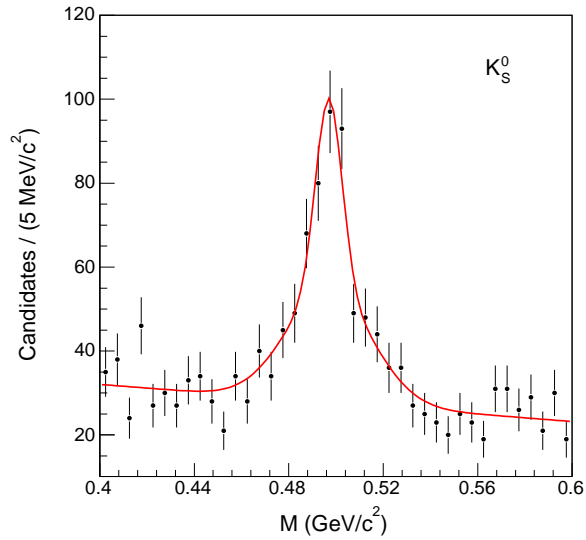


FIG. 8: Invariant mass distribution of K_S^0 candidates reconstructed using primary and additional muons. The line represents the fit described in the text.

After removing the predicted numbers of fake muons, the fraction of events with an identified K_S^0 meson that contain additional real muons is $(6.83 \pm 0.45)\%$. It is $(5.6 \pm 1.05)\%$ for events with an identified K^{*0} meson. The average of the two fractions is $(6.6 \pm 0.4)\%$. We multiply this fraction by the number of ghost events due to ordinary sources (241507 ± 10284) to predict the number of real muons in events due to heavy flavor that are classified as ghost events because one of the primary muons was produced by a pion or kaon in-flight-decay. This procedure yields a slight overestimate because, according to the simulation tuned with the data, $(53.4 \pm 0.4)\%$ of the $K \rightarrow \mu$ misidentifications are due to events with heavy flavors, whereas $(51.3 \pm 0.6)\%$ of the ghost events arise from heavy flavor production. As shown by Table X, the improved estimate still does not account for 12169 ± 1319 ghost events with additional real muons.

TABLE X: Number of additional muons in ghost events are compared to the number of expected fake muons and real muons from heavy flavor decays. The data correspond to an integrated luminosity of 1426 pb^{-1} .

Data	Fakes	K_S^0 second leg	Heavy Flavor
49142 ± 519	20902 ± 284	147 ± 15	15924 ± 1179

VIII. CONCLUSIONS

This article reports an improved understanding of the dimuon samples acquired by the CDF experiment. One dataset, corresponding to an integrated luminosity of 742 pb^{-1} , consists of 743006 events containing two central ($|\eta| < 0.7$) primary (or trigger) muons, each with transverse momentum $p_T \geq 3 \text{ GeV}/c$, and with invariant mass larger than $5 \text{ GeV}/c^2$ and smaller than $80 \text{ GeV}/c^2$. These data are split into two subsets: one, referred to as $P + HF$, consisting of 589015 ± 5074 events in which both muons originate inside the beam pipe of radius 1.5 cm; and one, referred to as ghost, consisting of 153991 ± 5074 events in which at least one muon originates beyond the beam pipe. The study in Ref. [4] shows that the number and properties of $P + HF$ events are correctly modeled by the expected contributions of semileptonic heavy flavor decays, prompt quarkonia decays, Drell-

Yan production, and instrumental backgrounds due to punchthrough of prompt or heavy-flavored hadrons which mimic a muon signal. A previous study [5] has investigated significant sources of ghost events, such as in-flight-decays of pions and kaons and hyperon decays. That study could account for approximately half of the ghost events but was unable to assess the uncertainty of the in-flight-decay prediction. The present study shows that the HERWIG parton-shower generator provides an accurate model of the data. The large discrepancy in the previous study was generated by not including the contribution of final states in which a $b(c)$ hadron decays semileptonically and the second muon is produced by the in-flight-decay of a particle in the recoiling jet. After tuning by a few percent the pion and kaon rates predicted by the simulation with a fit to the data, we show that ordinary sources, mostly in-flight-decays, account for 125665 ± 5351 of the 153991 ± 5074 ghost events isolated in the sample of 743006 dimuons.

For comparison, a D0 study has used a similar dimuon sample to set a limit [3] of $(0.4 \pm 0.26 \text{ stat} \pm 0.53 \text{ syst})\%$ to the fraction of muons produced at a distance larger than 1.6 cm from the beamline including pion and kaon in-flight-decays. This appears to be in contradiction with the present result, and also with a recent estimate [31] of the fraction of $K \rightarrow \mu$ and $\pi \rightarrow \mu$ contributions in the D0 subset of same-charge dimuons ($\simeq 40\%$).

The present study also improves a previous estimate [5] of the content of additional muons with $p_T \geq 2 \text{ GeV}/c$ and $|\eta| \leq 1.1$ in ghost events. We find that $(23 \pm 6)\%$ of the unaccounted ghost events contain additional real muons. For comparison, the fraction of $b\bar{b}$ events that contain additional muons due to sequential semileptonic decays is $(6.9 \pm 0.4)\%$.

Both results presented in this article have implications for measurements derived in dimuon datasets without properly accounting for the presence of ghost events. As an example, the measurement of the dimuon charge asymmetry performed by the D0 experiment [31] estimates the fraction of $K \rightarrow \mu$ and $\pi \rightarrow \mu$ misidentifications with a similar method. After removing this background, the remaining muon pairs with same charge are attributed to $b\bar{b}$ production. The present study shows that, after removing this type of misidentified muons, the data set still contains an additional component that cannot be accounted for with ordinary sources. The size of this component, equally split in opposite and same sign pairs [5], is $(12.8 \pm 3.2)\%$ of the total number of dimuons due to $b\bar{b}$ production.

IX. ACKNOWLEDGMENTS

We thank the Fermilab staff and the technical staffs of the participating institutions for their vital contributions. This work was supported by the U.S. Department of Energy and National Science Foundation; the Italian Istituto Nazionale di Fisica Nucleare; the Ministry of Education, Culture, Sports, Science and Technology of Japan; the Natural Sciences and Engineering Research Council of Canada; the National Science Council of the Republic of China; the Swiss National Science Foundation; the A.P. Sloan Foundation; the Korean World Class University Program, the National Research Foundation of Korea; the Science and Technology Facilities Council and the Royal Society, UK; the Institut National de Physique Nucleaire et Physique des Particules/CNRS; the Russian Foundation for Basic Research; the Ministerio de Ciencia e Innovación, and Programa Consolider-Ingenio 2010, Spain; the Slovak R&D Agency; the Academy of Finland; and the Australian Research Council (ARC).

-
- [1] F. Abe *et al.*, Phys. Rev. D **55**, 2546 (1997).
 - [2] D. Acosta *et al.*, Phys. Rev. D **69**, 012002 (2004).
 - [3] M. R. J. Williams, Fermilab-CONF-09-308-E, PosEPS 2009, 248 (2009).
 - [4] T. Aaltonen *et al.*, Phys. Rev. D **77**, 072004 (2008).
 - [5] T. Aaltonen *et al.*, arXiv:0810.5357, Eur. Phys. J. C **68**,109 (2010).
 - [6] F. Abe *et al.*, Nucl. Instrum. Methods Phys. Res., Sect. A **271**, 387 (1988).
 - [7] R. Blair *et al.*, Fermilab Report No. FERMILAB-Pub-96/390-E (1996).
 - [8] C. S. Hill *et al.*, Nucl. Instrum. Methods Phys. Res., Sect. A **530**, 1 (2004).
 - [9] A. Sill *et al.*, Nucl. Instrum. Methods Phys. Res., Sect. A **447**, 1 (2000).
 - [10] T. Affolder *et al.*, Nucl. Instrum. Methods Phys. Res., Sect. A **453**, 84 (2000).
 - [11] T. Affolder *et al.*, Nucl. Instrum. Methods Phys. Res., Sect. A **526**, 249 (2004).
 - [12] G. Ascoli *et al.*, Nucl. Instrum. Methods Phys. Res., Sect. A **268**, 33 (1988).
 - [13] J. Elias *et al.*, Nucl. Instrum. Methods Phys. Res., Sect. A **441**, 366 (2000).
 - [14] D. Acosta *et al.*, Nucl. Instrum. Methods Phys. Res., Sect. A **461**, 540 (2001).
 - [15] R. Downing *et al.*, Nucl. Instrum. Methods Phys. Res., Sect. A **570**, 36 (2007).
 - [16] M. M. Block and R. N. Cahn, Rev. Mod. Phys. **57**, 563 (1985).

- [17] S. Klimenko *et al.*, Fermilab Report No. FERMILAB-FN-0741 (2003).
- [18] The impact parameter is defined as the distance of closest approach of a track to the primary event vertex in the transverse plane with respect to the beamline.
- [19] That study follows the methodology of previous measurements that ignored other possible sources of muons. For example, muon tracks from pion and kaon in-flight-decays inside the tracking volume were regarded as prompt tracks because the track reconstruction algorithms were believed to remove decay muons with an appreciable kink.
- [20] B. Abbott *et al.*, Phys. Lett. B **487**, 264 (2000).
- [21] G. Apollinari *et al.*, Phys. Rev. D **72**, 072002 (2005).
- [22] G. Marchesini and B. R. Webber, Nucl. Phys. B **310**, 461 (1988); G. Marchesini *et al.*, Comput. Phys. Commun. **67**, 465 (1992).
- [23] D. J. Lange, Nucl. Instrum. Meth. A **462**, 152 (2001). We use version V00-14-05 downloaded from <http://www.slac.stanford.edu/BFR00T/dist/packages/EvtGen/>.
- [24] R. Brun *et al.*, CERN Report No. CERN-DD-78-2-REV; R. Brun *et al.*, CERN Programming Library Long Write-up W5013 (1993).
- [25] P. J. Sutton *et al.*, Phys. Rev. D **45**, 2439 (1992); P. J. Rijken and W. L. Van Nerven, Phys. Rev. D **51**, 44 (1995).
- [26] D. Acosta *et al.*, Phys. Rev. Lett. **88**, 161802 (2002).
- [27] M. L. Mangano, P. Nason, and G. Ridolfi, Nucl. Phys. **B373**, 295 (1992).
- [28] D. Acosta *et al.*, Phys. Rev. D **69**, 072004 (2004).
- [29] J. Nakamura *et al.*, J. Phys. G **37**, 075021 (2010).
- [30] F. James and M. Roos, Comput. Phys. Commun. **10**, 343 (1975).
- [31] V. M. Abazov *et al.*, Phys. Rev. D **82**, 032001 (2010).